JACS
JOURNAL OF THE AMERICAN CHEMICAL SOCIETY
pubs.acs.org/JACS
Article

Spatially Patterned Neutralizing Icosahedral DNA Nanocage for Efficient SARS-CoV-2 Blocking

Jialu Zhang,[‖] Yunyun Xu,[‖] Yihao Huang, Miao Sun, Siwen Liu, Shuang Wan, Honglin Chen, Chaoyong Yang, Yang Yang,* and Yanling Song*

Cite This: https://doi.org/10.1021/jacs.2c02764
Read Online

ACCESS | Metrics & More | Article Recommendations | Supporting Information

ABSTRACT: Broad-spectrum anti-SARS-CoV-2 strategies that can inhibit the infection of wild-type and mutant strains would alleviate their threats to global public health. Here, we propose an icosahedral DNA framework for the assembly of up to 30 spatially arranged neutralizing aptamers (IDNA-30) to inhibit viral infection. Each triangular plane of IDNA-30 is composed of three precisely positioned aptamers topologically matching the SARS-CoV-2 spike trimer, thus forming a multivalent spatially patterned binding. Due to its multiple binding sites and moderate size, multifaced IDNA-30 induces aggregation of viruses. The rigid icosahedron framework afforded by four helixes not only forms a steric barrier to prevent the virus from binding to the host but also limits the conformational transformation of the SARS-CoV-2 spike trimer. Combining multivalent topologically patterned aptamers with structurally well-defined nanoformulations, IDNA-30 exhibits excellent broad-spectrum neutralization against SARS-CoV-2, including almost completely blocking the infection of Omicron pseudovirus. Overall, this multidimensional neutralizing strategy provides a new direction for the assembly of neutralizing reagents to enhance their inhibitory effect against SARS-CoV-2 infection and combat other disease-causing viruses.

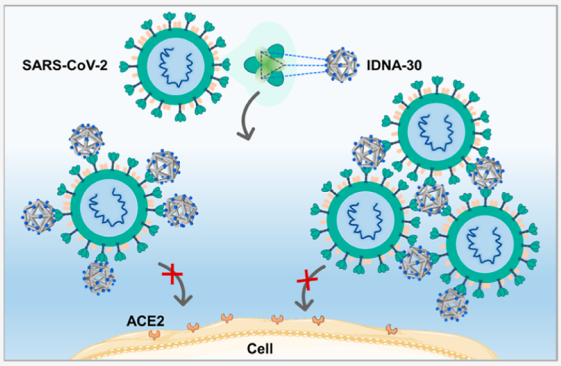

INTRODUCTION

To date, the SARS-CoV-2 virus has caused a global pandemic, and the constantly emerging new variants have posed challenges to prophylaxis and postexposure therapy. The SARS-CoV-2 virus hijacks the angiotensin-converting enzyme-2 (ACE2) of host cells by the spike trimer (S trimer) on the viral surface.[1] One promising approach to inhibit viral infection is the development of neutralizing reagents that block the interaction of S trimer-ACE2 with high efficacy, resulting in efficient inhibition of the SARS-CoV-2 invasion pathway. Most viruses engage with host cells by multivalent interactions, enabling efficient cell attachment and realization of the infection process. Furthermore, the spikes of most enveloped viruses are distributed at distinctive distances with specific geometric patterns, resulting in unique infection features.[2,3] The enormous enhancement of the natural interaction between receptors and ligands can be easily accomplished due to the more orderly and topological arrangements of multivalent ligands.[4] Therefore, topologically ordered multivalent neutralizing reagents have a high potential to improve the neutralization efficiency and resist mutational escape, compared to monovalent neutralization reagents.

However, the introduction of neutralizing antibodies in certain multivalent nanodevices causes cumbersome and time-consuming conjugate workflow.[5] Compared with the complicated customization modification of neutralizing antibodies, neutralizing aptamers, which are essentially nucleic acids, can be programed and assembled onto various nanodevices for scalable applications.[6] Moreover, aptamers exhibit distinctive advantages of low cost, low immunogenicity, and facile, controllable production with little batch-to-batch variation.[7] Recently we and other groups have identified several neutralizing agents against SARS-CoV-2, in the form of monovalent[8−13] and bivalent aptamers[14] and spherical aptamers[15] based on gold nanoparticles. The ability of topological control has rarely been realized, exhibiting unsatisfactory therapeutic efficacy or leading to the introduction of unnatural nanoscaffolds. Therefore, it is of utmost importance to develop a spatially matched neutralizing aptamer-based strategy against SARS-CoV-2 and its unknown mutants.

The programmability of DNA nanostructures offers delicate tools to precisely regulate other molecules in terms of number, location, and relative distance over space.[16−21] Furthermore,

Received: March 14, 2022

ACS Publications
© XXXX American Chemical Society

https://doi.org/10.1021/jacs.2c02764
J. Am. Chem. Soc. XXXX, XXX, XXX−XXX

Scheme 1. Spatially Matched Multisite Locking Strategy of IDNA-30 against SARS-CoV-2[a]

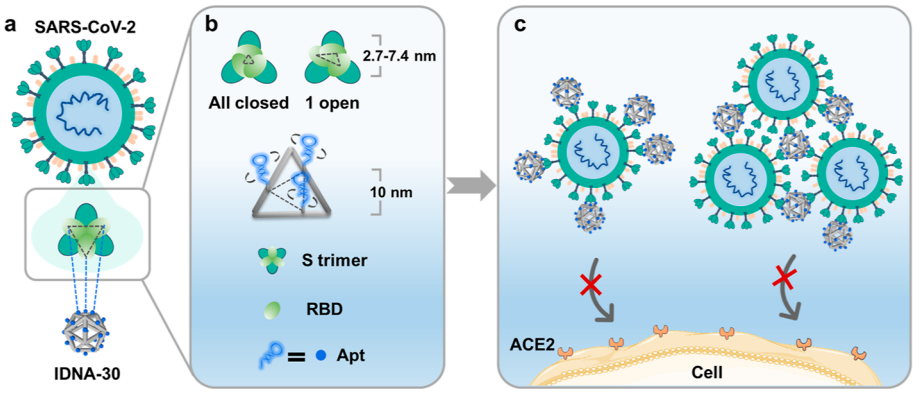

[a]The distances between different monomers of the S trimer change with the open state of the RBD. Even though the spacing of aptamers on the same plane is ca. 10 nm, the extended area of the aptamer fluctuates by ca. 10 nm. Additionally, there may be several possible binding modes when adjacent subunits or adjacent proteins combine with aptamers.

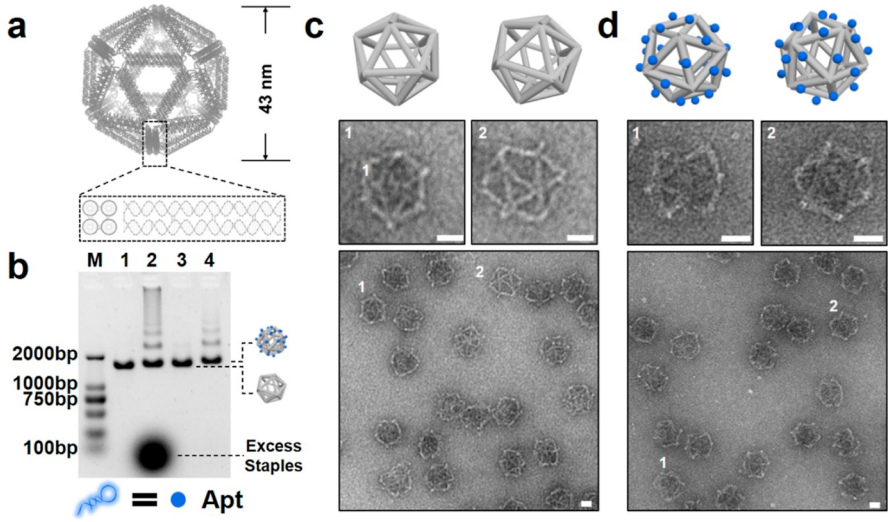

Figure 1. Design and characterization of ID and IDNA-30. (a) three-dimensional cartoon model of ID. ID has a rigid frame configuration owing to the bundle of 4 helixes bundle on each side. (b) 1.5% Agarose gel electrophoresis analysis of DNA nanostructures (lane 1: scaffold 7560, lane 2: unpurified ID, lane 3: ID, and lane 4: IDNA-30). TEM images of (c) ID and (d) IDNA-30. IDNA-30 was obtained by the orderly arrangement of aptamers on ID. Scale bar = 20 nm.

spatially arranged molecules may work collectively or associatively to achieve better efficiency compared to a disordered array.[22] Moreover, due to the biocompatible nature of DNA, aptamer-integrated DNA nanostructures minimize the adverse effects of the introduction of other unnatural scaffolds. Therefore, a DNA nanodevice equipped with neutralizing aptamers in a precise pattern may be promising for the realization of a SARS-CoV-2 blockade. Considering the features of the SARS-CoV-2 S trimer and its infection mechanism,[23] we employed an icosahedral DNA origami framework to present SARS-CoV-2 neutralizing aptamers with specifically assigned numbers and spatial locations to block the interaction between the S trimer and host ACE2 (Scheme 1a).

RESULTS AND DISCUSSION

Design and Characterization of Neutralizing Icosahedral DNA Nanocage. Considering the triangular pattern of the S trimer, as a regular polyhedron with the most equilateral triangular faces, an icosahedral DNA origami was prototyped to carry n neutralizing aptamers (termed IDNA-*n*, $n \leq 30$). First, IDNA-*n* can serve as an isotropic nanoparticle with 20 equilateral triangular faces holding 0−3 blocking agents on each face (ca. 10 nm) against the S trimer (~13 nm in diameter[24]). In addition, by virtue of the relatively excellent molecular flexibility of the toehold sequence (~7 nm), IDNA-n provides an accessible molecular handle to trap receptor binding domains (RBDs) (Scheme 1b), circumventing the size fluctuations resulting from conformational transitions of RBDs in the S trimer[25] (2.7−7.4 nm, Figure S1). For complete decoration, through complementary strand hybridization, each triangular plane of IDNA-30 equips three precisely located aptamers topologically matched with the spike trimer of SARS-CoV-2. As a result, by combining the topologically matched aptamer trimers and flexible DNA connectors, IDNA-30 can boost binding affinity and neutralization efficacy, avoiding the potential dissociation of single-point inhibition. Second, multi-faced IDNA-30 could potentially induce aggregation of viruses due to multivalent binding and its moderate size, which can slow the movement of viruses and, thus, further reduce SARS-CoV-2 infection (Scheme 1c). Third, the rigid framework afforded by four helixes on each side not only provides a steric barrier for S

https://doi.org/10.1021/jacs.2c02764
J. Am. Chem. Soc. XXXX, XXX, XXX−XXX

trimer-ACE2 interaction but also limits S trimer conformational transformation, thus further inhibiting viral membrane fusion. More importantly, the neutralizing aptamers display a relatively compact arrangement and prevent accessibility by nuclease, reducing the degradation of DNA. Therefore, combining multivalent topologically patterned aptamers with structurally well-defined nanoformulations, IDNA-30 is capable of inhibiting SARS-CoV-2 infection at multiple levels, enhancing the therapeutic efficacy.

As shown in Figures 1a and S2, the icosahedral DNA framework (possessing 12 vertices, 30 edges, and 20 faces) was designed via the software Tiamat and constructed by a 7560nt scaffold and 216 staples. Different from the reported icosahedral DNA origami with double-helix edges,[16] our edges were intentionally designed as four-helix bundles (63nt, ~21 nm in length; 5 nm in thickness) to achieve enhanced structural rigidity and stability[26] (Supplementary Video). Considering this DNA icosahedron as a bilayer of the double-helix framework, staples at the vertices were tailored to generate unbalanced tensions at the outer and inner layer and assure the unique wrapping topology; therefore, aptamers were guaranteed to be present at only the outer surface. Compared with disordered and uncertain multivalent recognition, this distinctive structure provided more unequivocal areas for receptor-ligand recognition, achieving more efficient binding.

By virtue of the high programmability of DNA nanostructures, neutralizing aptamers with elongated anti-toehold sequences could be immobilized at the assigned toehold sites on the edges to achieve a controllable pattern. In the case of a fully decorated frame IDNA-30, the flexibility provided by the 21bp (~7 nm) toehold pairs allowed the neutralizing aptamers to wander and offer relatively dynamic locking patterns against the S trimers. Because the theoretical distance between adjacent S1 subunits of the S trimer changes by 2.7−7.4 nm with the conformational transition of RBD, three coplanar aptamers were able to provide more compact binding sites to attack one S trimer. Meanwhile, the peripheral neutralizing aptamers were still available to grab surrounding S trimers to enhance the binding, while the remote neutralizing aptamers were also free to bind and lock onto another virus particle (Scheme 1).

First, ID was acquired by thermal annealing of numerous single-stranded DNA (Tables S1−S3) and purified by rate-zonal centrifugation. Compared with ID, the decreased mobility of IDNA-30 in agarose gel electrophoresis (AGE) indicated successful assembly of neutralizing aptamers (Figure 1b). Transmission electron microscopy (TEM) imaging further demonstrated the topology and size of the well-composed ID, which were in accordance with the theoretical design (Figures 1c and S3). IDNA-30 maintained the same formation and dispersion (Figure 1d). Moreover, IDNA-30 showed outstanding structural integrity after even 35 days of storage at 4 °C (Figure S4). To evaluate the stability of IDNA-30 against nuclease degradation in a biological matrix, IDNA-30 was incubated with DMEM cell media with 10% fetal bovine serum at 37 °C for several hours. The bands from the AGE image showed that the IDNA-30 remained sufficiently stable even after 48 h incubation (Figure S5). Additionally, IDNA-30 displayed binding capability against SARS-CoV-2 RBD after being pretreated with fetal bovine serum for 3 h (Figure S6) or stored at 4 °C for 7 days (Figures S7 and S8). IDNA-30 also showed superior binding ability against RBD in saliva with about a five-fold signal-background ratio (Figure S9). This stability is likely due to the dense spatial arrangement of aptamers in IDNA-30, as well as the inherent electronegativity and nick-hidden strands of ID. Such excellent stability of IDNA-30 indicates its promise as a foundation for subsequent applications in complex biological systems.

Study of the Binding Mode of SARS-CoV-2 Pseudovirus with IDNA-30. Next, we investigated the interaction between virions and IDNA-30 by imaging experiments. Cryo-EM images showed S trimers with a nail-like shape embedded in the envelope of SARS-CoV-2 pseudovirus, consistent with a previous study of authentic SARS-CoV-2[27] (Figures 2a and S10). Each IDNA-30 binds to more than one spike trimer in a single virus (Figure 2a, up), and also can serve as a connector to form a poly-viral complex (Figure 2a, bottom), suggesting the role of multivalent receptor-ligand interaction. In detail, the aptamers of IDNA-30 are bound with the S trimers and provide steric hindrance against receptor binding (Figure S11). Therefore, this face-to-face blocking strategy not only achieves spatial multisite synergy but also has the potential to deal with

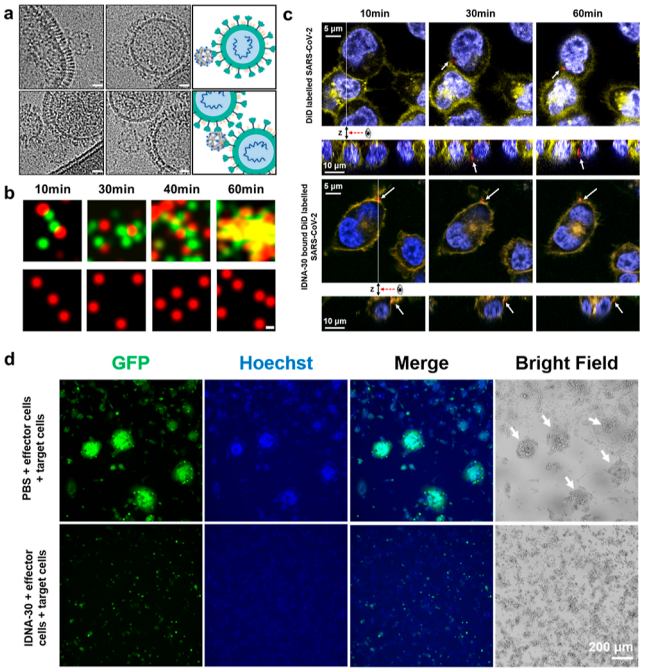

Figure 2. Characterization of the binding mode of SARS-CoV-2 pseudovirus with IDNA-30. (a) Cryo-electron microscopy (cryo-EM) of SARS-CoV-2 pseudovirus bound with IDNA-30. Scale bar = 20 nm. (b) Different time points of selected confocal frames from top row: virus particles (red) incubated with IDNA-30 (green) and bottom row: virus particles (red) at room temperature. Scale bar = 1 μm. (c) Confocal imaging. Top row: viral accumulation over time for the no-inhibitor treated condition. Bottom row: viral entry inhibition over time during IDNA-30 treatment. An eye symbol of cross-sections at each time point represents the observation direction (along the dotted lines in the abovementioned images). The cross-sections were reconstructed from Z stacks with twenty images taken at different focal planes (spacing: 1 μm). Cell nuclei (blue), cell membrane (yellow), and virus (red) were stained with Hoechst, DiI, and DiD, respectively. The white arrows point to representative viral particles. (d) Representative images of 293T-SARS-CoV-2-Spike-Del18-HA-OE(GFP) cells pretreated without or with 15 nM IDNA-30 before co-culturing with ACE2-transfected HEK293T cells for 48 h are displayed. The white arrows point to representative syncytium formation. 293T-SARS-CoV-2-Spike-Del18-HA-OE(GFP) and ACE2-transfected HEK293T cells were defined as effector cells and target cells, respectively.

https://doi.org/10.1021/jacs.2c02764
J. Am. Chem. Soc. XXXX, XXX, XXX−XXX

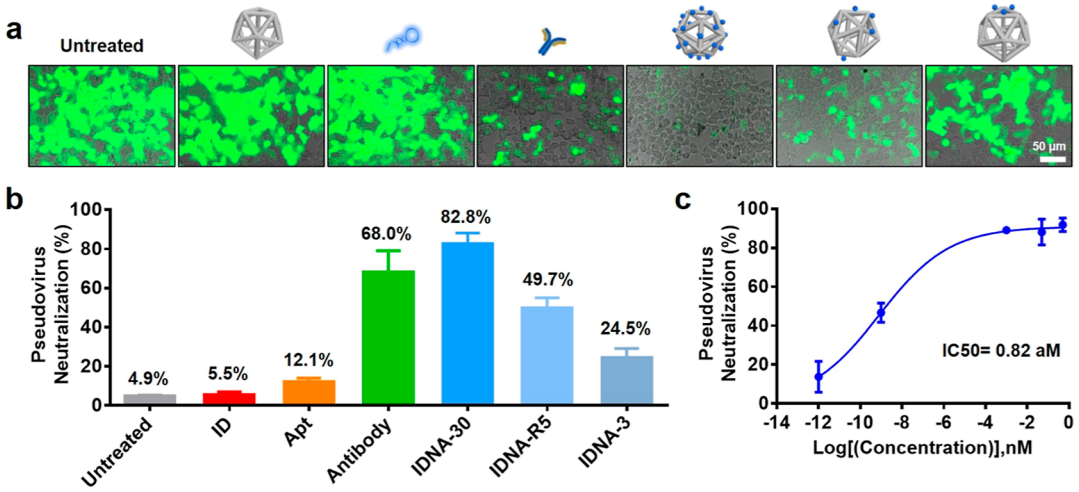

Figure 3. Assessment of pseudotyped SARS-CoV-2 neutralization assay. (a) Fluorescence images and (b) bar graph of infection efficiency for SARS-CoV-2 pseudovirus treated with 1 nM ID, Apt, Antibody, IDNA-30, IDNA-R5, and IDNA-3. IDNA-3 and IDNA-30 were engineered with a deterministic arrangement, while IDNA-R5 was functionalized with aptamers randomly. The IDNA-N concentration was the corresponding concentration of IDNA. (c) Pseudovirus neutralization curve of IDNA-30.

antigenic drift through spatial multisite locking to interrupt subsequent viral invasion.

Two primary binding modes can be speculated based on different ratios of particle concentration of virions incubated with IDNA-30 (Figure S12). On one hand, even though S trimers are distributed randomly and sparsely on the surface of SARS-CoV-2,[27] in the case of (locally) low IDNA-30 to virion ratio, IDNA-30 can serve as a connector, resulting in aggregation of virions, which can slow the mobility rate of SARS-CoV-2. On the other hand, at (locally) high IDNA-30 to virion ratio, some virions are covered with IDNA-30, termed "dreamcatcher", which reduces the accessibility to host receptors. Confocal images of unbound or IDNA-30-bound virions with the same order of magnitude particle concentration were consistent with the results of cryo-EM and TEM (Figures 2b and S12). The aggregation phenomenon emerged gradually after virions were incubated with a particle concentration of 2.5 times IDNA-30 at room temperature for 30 min (Figures 2b and S13). Remarkably, IDNA-30-bound virions exhibit marked size expansion compared to free virions. Due to the increase of mass, the larger nanoparticles display a lower range of movement with slow mobility based on the Brownian motion principle.

To further explore the SARS-CoV-2 infection, we tracked the entry of DiD-labeled SARS-CoV-2 pseudovirus into the host cells by time-lapsed confocal imaging. Compared to unbound virions, IDNA-30-bound virions flowed on the cell membrane, reducing the binding of virions and cells, and even decreasing the opportunity of entering cells over time (Figures 2c and S14). Two main reasons are speculated to explain this phenomenon. On one hand, larger complexes block the mobility of IDNA-30-bound virions when they were introduced to cells. On the other hand, considering negative charges from both DNA backbone and virion surface proteins, viral entry inhibition may be ascribed to the enhanced electrostatic repulsion between the host cell and IDNA-30-bound virions. Additionally, there was no obvious cell internalization even after incubation of IDNA-30 with cells at 37 °C for 4 h (Figure S15). Quantitative assay by flow cytometry corroborated these results (Figure S16).

Moreover, we speculated another underlying mechanism that IDNA-30 could interrupt the membrane fusion of SARS-CoV-2 spike-expressing cells and ACE2-expressing host cells. As the energy-driven postfusion conformation is irreversible, the infection process would be blocked for premature activation of S trimer's conformational changes for fusion.[28] Therefore, we constructed HEK293T cells expressing the SARS-CoV-2 Spike-Del18 protein and ZsGreen on the cell membrane (effector cells) to obtain a macroscopic perspective of the receptor-ligand-mediated cell−cell fusion. After mixing the effector cells and ACE2-expressing HEK293T cells (target cells) at an equivalent ratio, SARS-CoV-2 S trimers could trigger ACE2-related membrane fusion without the inhibition of IDNA-30, consistent with the plasma membrane fusion pathway of SARS-CoV-2 reported previously[28] (Figures 2d and S17). The syncytium formation and weaker fluorescence intensity of fused cells indicated the successful establishment of infection. However, in the presence of IDNA-30, the decreased syncytium revealed that cell−cell fusion tendency was significantly weakened. In light of the abovementioned underlying mechanism, IDNA-30 holds promise as an alternate SARS-CoV-2 neutralizing reagent, rather than neutralization by the aptamer itself.

In vitro SARS-CoV-2 Pseudovirus Inhibition. Next, to demonstrate the inhibition of pseudovirus infection by IDNA-30, we carried out a neutralization assay as displayed in Figure S18. Owing to the multivalent collaboration and steric barrier caused by IDNA-30, the neutralizing efficiency of IDNA-30 (82.8%) was ~7 times higher than the monomer aptamer's efficiency (12.1%) (Figure 3b, Apt). To demonstrate the advantages of multivalent topologically patterned IDNA-30, we designed two IDNA-N control groups, IDNA-3 (three aptamers with coplanar precise distribution pattern, Figure S2, Table S1, S2, S4) and IDNA-R5 (five aptamers with random distribution pattern, Figure S2). Neutralization by IDNA-30 exhibited much higher potency than those of IDNA-3 (24.5%) and IDNA-R5 (49.7%) (Figure 3b) at the same structure concentration, suggesting that the arrangement with higher density and more number aptamers of IDNA-30 provides effective inhibition of viral infection. Additionally, even with the same numbers of aptamers, the neutralizing ability of single-stranded DNA with three aptamers (TriApLinear, 27.0%) against pseudovirus was inferior to those of IDNA-30 (82.8%) and tetrahedron DNA nanostructure engineered with precisely positioned three

https://doi.org/10.1021/jacs.2c02764
J. Am. Chem. Soc. XXXX, XXX, XXX−XXX

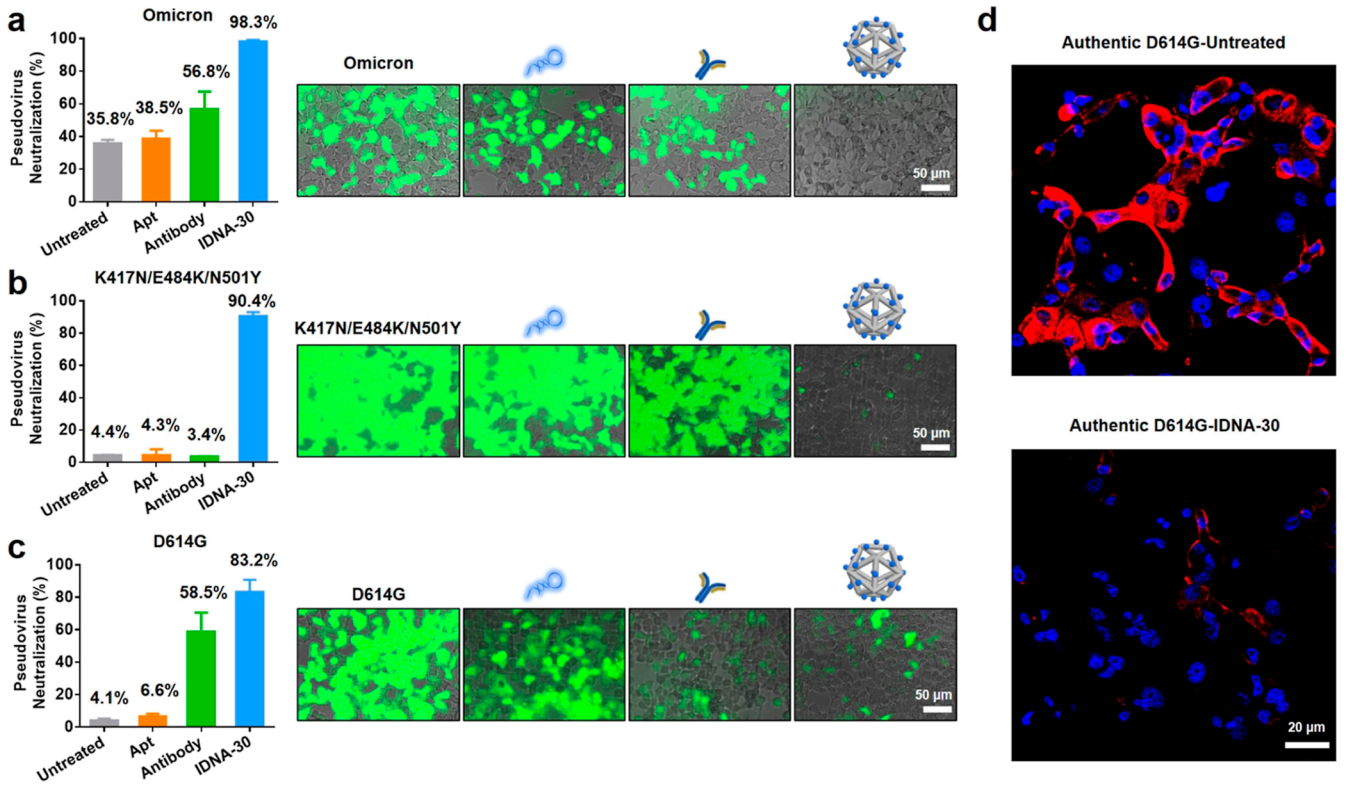

Figure 4. Assessment of mutant pseudotyped and authentic SARS-CoV-2 neutralization assay. (a) Fluorescence bar graphs and neutralization potency of pseudovirus SARS-CoV-2 (Omicron) treated with 15 nM Apt, Antibody, and IDNA-30. (b) Fluorescence bar graphs and neutralization potency of pseudovirus SARS-CoV-2 with K417N/E484K/N501Y mutations treated with 10 nM Apt, Antibody, and IDNA-30. (c) Fluorescence images and neutralization potency of 5 nM Apt, Antibody, and IDNA-30 that target the pseudovirus SARS-CoV-2 with D614G mutation. (d) Images of IDNA-30 neutralization of authentic SARS-CoV-2 with D614G variant infection of Vero E6 cells. Up: Untreated; Bottom: 10 pM IDNA-30. The fixed cells were stained with Hoechst dye (blue) for the cell nucleus and an anti-SARS-CoV-2 nucleocapsid antibody (red) for the virus.

aptamers (TriApTDN, 81.1%) (Figures S19 and S21a, Table S5). Such superior neutralization of IDNA-30 and TriApTDN might be ascribed to spatially patterned blocking and the steric hindrance caused by the rigid stereoscopic framework.

Moreover, at the same concentration, a commercial neutralizing antibody (Research Resource Identifiers number: AB_2857935) showed inferior neutralization (68.0%) (Figure 3b). Instead of the infectious cell count in the images shown in Figure 3a, measurement based on the overall fluorescence intensity, neutralized pseudovirus SARS-CoV-2 exhibited a half-maximal inhibitory concentration (IC_{50}) of 0.82 aM, corresponding to an inhibitory ability of 91.9% (Figure 3c), indicating superior neutralization compared to previous antibody-based neutralization (Table S6), bivalent aptamer,[14] and the aptamer-modified gold nanoparticles.[15] Collectively, by exploiting the spatial multisite locking and rigid framework blocking, IDNA-30 is an alternative neutralizing nanoreagent for SARS-CoV-2.

In vitro Mutant Pseudotyped and Authentic SARS-CoV-2 Inhibition. The evolution of SARS-CoV-2 is raising broad concern, not only due to enhanced infectiousness but also because the unlimited mutations could weaken the effectiveness of certain neutralization antibodies or vaccines.[29] New variants tend to display the accumulation of multiple mutations to cope with a changeable environment. Although the aptamer can still bind to Omicron RBD (Figure S20), neither TriApTDN (55.5%) nor TriApLinear (38.0%) displayed an effective neutralization against Omicron pseudovirus (Figure S21b). Remarkably, IDNA-30 displayed delightful neutralization against Omicron pseudovirus with over 98.0% neutralization efficiency (Figure 4a), having the potential to overcome the dilemma that Omicron escapes the majority of existing SARS-CoV-2 neutralizing antibodies.[29] This might be attributed to more spatially patterned aptamers introduced by IDNA-30 to block collaboratively, which better compensates for the decrease of monomer aptamer's affinity caused by clustered mutations on Omicron.[30]

Subsequently, we further probed the cases of the single mutant (D614G) and triple mutant (K417N/E484K/N501Y), which have played pivotal roles in the viral invasion of SARS-CoV-2 variants.[31] As expected, the inhibition ability of a monomer aptamer was negligible in both cases, verifying the limitations of single-point blocking encountered off-target. Even with three aptamers, TriApLinear and TriApTDN displayed inferior neutralizing effects against triple mutant pseudovirus (Figures S21c). Moreover, the antibody exhibited relatively reduced efficiency of neutralization against a single mutant (Figures 4c), and almost complete loss of neutralizing effect against multiple mutants (Omicron) (Figure 4a) and a triple mutant (Figure 4b). This may be attributed to the antigen drift. In contrast, IDNA-30 still demonstrated high potency against a single mutant with 83.2% and a triple mutant with 90.4% neutralization efficiency (Figure 4b,c).

With collaborative recognition by multivalent aptamers, larger IDNA-30-bound virus complexes showed hindered invasion speed. Simultaneously, the steric barriers caused by IDNA-30 blocked subsequent membrane fusion. It is also striking that 10 pM IDNA-30 displayed potent neutralization potency (85.5%) against the authentic virions with D614G mutation (GenBank:

https://doi.org/10.1021/jacs.2c02764
J. Am. Chem. Soc. XXXX, XXX, XXX−XXX

MT835143.1) (Figure 4d). As previously reported, different expression levels of spike protein and infection mechanisms may lead to different neutralization effects of pseudovirus and authentic viruses.[32−34] Additionally, compared with the untreated group, the fluorescence intensity of infectious cells of IDNA-30 was relatively dim, suggesting that fusion of virus and host membrane was prevented by IDNA-30. Cumulative evidence shows that IDNA-30 exhibits excellent and robust neutralization and has outstanding potential in developing novel prophylaxis and therapeutic strategies to confront the COVID-19 pandemic.

Finally, the safety of IDNA-30 was tested. Although any foreign molecule may cause potential immunogenicity, DNA nanostructures, in general, exhibit minimal toxicity, superior biocompatibility, and low immunogenicity.[35−37] As expected, the cytotoxicity of IDNA-30 was undetectable, even at a concentration of 10 nM (Figure S22). Moreover, there was no white blood cell response to IDNA-30 (Figure S23), negligible change in the cytokine level of mouse plasma (Figure S24), and normal histological results (Figure S25), demonstrating that IDNA-30 is immunologically inert, which is conducive to the development of subsequent practical applications.

CONCLUSIONS

In summary, we designed an icosahedral DNA framework as a rigid scaffold that is functionalized by neutralizing aptamers in a controllable fashion to achieve spatially multisite binding for inhibition of SARS-CoV-2 infection. Although many kinds of icosahedra have been developed previously,[16,38] an icosahedron with four helixes per side showed much higher structural homogeneity, which provides ligands with more unequivocal spatial pattern recognition domains. First, benefiting from the rigid framework and high programmability, IDNA-30 displayed excellent inhibitory ability by disrupting the process, which the virus hijacks the host cellular receptor. Compared with a disorderly group collaboration of aptamers, multiple aptamers of the IDNA-30 are expected to achieve more efficient neutralization in a controlled arrangement. Second, the spatial multisite locking and steric hindrance by IDNA-30 facilitated the inhibition of aptamers against the virus. The confined conformational shift of S trimers shown by cell−cell fusion indicates the broader neutralization by IDNA-30. Third, the clusters formed by IDNA-30-bound viruses displayed slow mobility during the infection process, possibly providing a responsive window period for immune cells. Furthermore, considering the excellent biocompatibility and biostability of DNA nanostructures[35,36,39] and no obvious cytotoxicity of IDNA-30, the clinical advance of this spatially patterned neutralizing strategy could be accelerated after subsequently evaluating the antiviral efficiency of IDNA-30 against Omicron in vivo via intranasal/pulmonary delivery or injection similar to neutralizing antibody (subcutaneous injection/intravenous injection/intraperitoneal injection/multiple combined ways).[40−42]

Overall, this programmable aptamer-integrated DNA nanostructure provides an excellent choice for the prophylaxis and postexposure therapy of SARS-CoV-2 or other viruses and pathogens with defined antigen structures. Given the distinctive structures and infectious mechanisms of various viruses, we expect that more matched aptamers and customized DNA nanostructures will be integrated to combat other viruses in the future.

ASSOCIATED CONTENT

Supporting Information

The Supporting Information is available free of charge at https://pubs.acs.org/doi/10.1021/jacs.2c02764.

Experimental materials; DNA sequence design; preparation and characterization of the ID and IDNA; preparation of TriApTDN and TriApLinear; stability analysis of DNA nanostructures TEM imaging and Cryo-EM analysis; preparation of DiD-labeled SARS-CoV-2 pseudovirus particles; confocal imaging cell-cell fusion assay; in vitro pseudotyped SARS-CoV-2 neutralization; authentic SARS-CoV-2 (D614G mutant) neutralization assay; enhanced cell counting kit-8 (cck-8) assays for cytotoxicity evaluation; flow cytometry analysis of leukocytes and ACE2-transfected HEK293T cells; and Flow cytometry analysis of the binding affinity of IDNA-30, RBD-beads CoV2-6C3 aptamer (Apt), and Omicron RBD-beads (PDF)

DNA icosahedron structure rendered by the software Tiamat (MP4)

AUTHOR INFORMATION

Corresponding Authors

Yang Yang − *Institute of Molecular Medicine and Shanghai Key Laboratory for Nucleic Acid Chemistry and Nanomedicine, State Key Laboratory of Oncogenes and Related Genes, Renji Hospital, School of Medicine, Shanghai Jiao Tong University, Shanghai 200127, China;* orcid.org/0000-0002-2630-6062; Email: yang.yang.nano@sjtu.edu.cn

Yanling Song − *The MOE Key Laboratory of Spectrochemical Analysis and Instrumentation, the Key Laboratory of Chemical Biology of Fujian Province, State Key Laboratory of Physical Chemistry of Solid Surfaces, Department of Chemical Biology, College of Chemistry and Chemical Engineering, Xiamen University, Xiamen 361005, China;* orcid.org/0000-0002-6793-6685; Email: ylsong@xmu.edu.cn

Authors

Jialu Zhang − *The MOE Key Laboratory of Spectrochemical Analysis and Instrumentation, the Key Laboratory of Chemical Biology of Fujian Province, State Key Laboratory of Physical Chemistry of Solid Surfaces, Department of Chemical Biology, College of Chemistry and Chemical Engineering, Xiamen University, Xiamen 361005, China; Institute of Molecular Medicine and Shanghai Key Laboratory for Nucleic Acid Chemistry and Nanomedicine, State Key Laboratory of Oncogenes and Related Genes, Renji Hospital, School of Medicine, Shanghai Jiao Tong University, Shanghai 200127, China*

Yunyun Xu − *Institute of Molecular Medicine and Shanghai Key Laboratory for Nucleic Acid Chemistry and Nanomedicine, State Key Laboratory of Oncogenes and Related Genes, Renji Hospital, School of Medicine, Shanghai Jiao Tong University, Shanghai 200127, China*

Yihao Huang − *The MOE Key Laboratory of Spectrochemical Analysis and Instrumentation, the Key Laboratory of Chemical Biology of Fujian Province, State Key Laboratory of Physical Chemistry of Solid Surfaces, Department of Chemical Biology, College of Chemistry and Chemical Engineering, Xiamen University, Xiamen 361005, China*

Miao Sun − *The MOE Key Laboratory of Spectrochemical Analysis and Instrumentation, the Key Laboratory of Chemical*

Biology of Fujian Province, State Key Laboratory of Physical Chemistry of Solid Surfaces, Department of Chemical Biology, College of Chemistry and Chemical Engineering, Xiamen University, Xiamen 361005, China

Siwen Liu − *State Key Laboratory for Emerging Infectious Diseases and InnoHK Centre for Infectious Diseases, Department of Microbiology, Li Ka Shing Faculty of Medicine, University of Hong Kong, Hong Kong SAR 999077, China*

Shuang Wan − *The MOE Key Laboratory of Spectrochemical Analysis and Instrumentation, the Key Laboratory of Chemical Biology of Fujian Province, State Key Laboratory of Physical Chemistry of Solid Surfaces, Department of Chemical Biology, College of Chemistry and Chemical Engineering, Xiamen University, Xiamen 361005, China*

Honglin Chen − *State Key Laboratory for Emerging Infectious Diseases and InnoHK Centre for Infectious Diseases, Department of Microbiology, Li Ka Shing Faculty of Medicine, University of Hong Kong, Hong Kong SAR 999077, China*

Chaoyong Yang − *The MOE Key Laboratory of Spectrochemical Analysis and Instrumentation, the Key Laboratory of Chemical Biology of Fujian Province, State Key Laboratory of Physical Chemistry of Solid Surfaces, Department of Chemical Biology, College of Chemistry and Chemical Engineering, Xiamen University, Xiamen 361005, China; Institute of Molecular Medicine and Shanghai Key Laboratory for Nucleic Acid Chemistry and Nanomedicine, State Key Laboratory of Oncogenes and Related Genes, Renji Hospital, School of Medicine, Shanghai Jiao Tong University, Shanghai 200127, China;* orcid.org/0000-0002-2374-5342

Complete contact information is available at: https://pubs.acs.org/10.1021/jacs.2c02764

Author Contributions

‖The authors J.Z. and Y.X. contributed equally to this work.

Notes

The authors declare no competing financial interest.

■ ACKNOWLEDGMENTS

We thank the Ministry of Science and Technology of China (2018YFA0902600), the National Natural Science Foundation of China (22022409, 21735004, 21874089, and 21977069), the Program for Changjiang Scholars, Innovative Research Team in University (IRT13036), and Innovative Research Team of High-Level Local Universities in Shanghai (SHSMU-ZLCX20212602).

■ REFERENCES

(1) Yan, R.; Zhang, Y.; Li, Y.; Xia, L.; Guo, Y.; Zhou, Q. Structural basis for the recognition of SARS-CoV-2 by full-length human ACE2. *Science* **2020**, *367*, 1444−1448.

(2) Marsh, M.; Helenius, A. Virus entry: open sesame. *Cell* **2006**, *124*, 729−740.

(3) Belouzard, S.; Millet, J. K.; Licitra, B. N.; Whittaker, G. R. Mechanisms of coronavirus cell entry mediated by the viral spike protein. *Viruses* **2012**, *4*, 1011−1033.

(4) Pan, L.; Fu, T.-M.; Zhao, W.; Zhao, L.; Chen, W.; Qiu, C.; Liu, W.; Liu, Z.; Piai, A.; Fu, Q.; Chen, S.; Wu, H.; Chou, J. J. Higher-Order Clustering of the Transmembrane Anchor of DR5 Drives Signaling. *Cell* **2019**, *176*, 1477−1489.

(5) Madsen, M.; Gothelf, K. V. Chemistries for DNA Nanotechnology. *Chem. Rev.* **2019**, *119*, 6384−6458.

(6) Meng, H.-M.; Liu, H.; Kuai, H.; Peng, R.; Mo, L.; Zhang, X.-B. Aptamer-integrated DNA nanostructures for biosensing, bioimaging and cancer therapy. *Chem. Soc. Rev.* **2016**, *45*, 2583−2602.

(7) Peinetti, A.; Lake, R.; Cong, W.; Cooper, L.; Wu, Y.; Ma, Y.; Pawel, G.; Toimil-Molares, M.; Trautmann, C.; Rong, L.; Mariñas, B.; Azzaroni, O.; Lu, Y. Direct detection of human adenovirus or SARS-CoV-2 with ability to inform infectivity using DNA aptamer-nanopore sensors. *Sci. Adv.* **2021**, *7*, No. eabh2848.

(8) Song, Y.; Song, J.; Wei, X.; Huang, M.; Sun, M.; Zhu, L.; Lin, B.; Shen, H.; Zhu, Z.; Yang, C. Discovery of Aptamers Targeting the Receptor-Binding Domain of the SARS-CoV-2 Spike Glycoprotein. *Anal. Chem.* **2020**, *92*, 9895−9900.

(9) Liu, X.; Wang, Y. L.; Wu, J.; Qi, J.; Zeng, Z.; Wan, Q.; Chen, Z.; Manandhar, P.; Cavener, V. S.; Boyle, N. R.; Fu, X.; Salazar, E.; Kuchipudi, S. V.; Kapur, V.; Zhang, X.; Umetani, M.; Sen, M.; Willson, R. C.; Chen, S. H.; Zu, Y. Neutralizing Aptamers Block S/RBD-ACE2 Interactions and Prevent Host Cell Infection. *Angew. Chem., Int. Ed.* **2021**, *60*, 10273−10278.

(10) Schmitz, A.; Weber, A.; Bayin, M.; Breuers, S.; Fieberg, V.; Famulok, M.; Mayer, G. A SARS-CoV-2 Spike Binding DNA Aptamer that Inhibits Pseudovirus Infection by an RBD-Independent Mechanism**. *Angew. Chem., Int. Ed.* **2021**, *60*, 10279−10285.

(11) Valero, J.; Civit, L.; Dupont, D. M.; Selnihhin, D.; Reinert, L. S.; Idorn, M.; Israels, B. A.; Bednarz, A. M.; Bus, C.; Asbach, B.; Peterhoff, D.; Pedersen, F. S.; Birkedal, V.; Wagner, R.; Paludan, S. R.; Kjems, J. A serum-stable RNA aptamer specific for SARS-CoV-2 neutralizes viral entry. *Proc. Natl. Acad. Sci. U.S.A.* **2021**, *118*, No. e2112942118.

(12) Yang, G.; Li, Z.; Mohammed, I.; Zhao, L.; Wei, W.; Xiao, H.; Guo, W.; Zhao, Y.; Qu, F.; Huang, Y. Identification of SARS-CoV-2-against aptamer with high neutralization activity by blocking the RBD domain of spike protein 1. *Signal Transduct. Targeted Ther.* **2021**, *6*, 227.

(13) Alves Ferreira-Bravo, I.; DeStefano, J. J. Xeno-Nucleic Acid (XNA) 2'-Fluoro-Arabino Nucleic Acid (FANA) Aptamers to the Receptor-Binding Domain of SARS-CoV-2 S Protein Block ACE2 Binding. *Viruses* **2021**, *13*, 1983.

(14) Sun, M.; Liu, S.; Wei, X.; Wan, S.; Huang, M.; Song, T.; Lu, Y.; Weng, X.; Lin, Z.; Chen, H.; Song, Y.; Yang, C. Aptamer Blocking Strategy Inhibits SARS-CoV-2 Virus Infection. *Angew. Chem., Int. Ed.* **2021**, *60*, 10266−10272.

(15) Sun, M.; Liu, S.; Song, T.; Chen, F.; Zhang, J.; Huang, J.-a.; Wan, S.; Lu, Y.; Chen, H.; Tan, W.; Song, Y.; Yang, C. Spherical Neutralizing Aptamer Inhibits SARS-CoV-2 Infection and Suppresses Mutational Escape. *J. Am. Chem. Soc.* **2021**, *143*, 21541−21548.

(16) Veneziano, R.; Moyer, T. J.; Stone, M. B.; Wamhoff, E.-C.; Read, B. J.; Mukherjee, S.; Shepherd, T. R.; Das, J.; Schief, W. R.; Irvine, D. J.; Bathe, M. Role of nanoscale antigen organization on B-cell activation probed using DNA origami. *Nat. Nanotechnol.* **2020**, *15*, 716−723.

(17) Kwon, P. S.; Ren, S.; Kwon, S.-J.; Kizer, M. E.; Kuo, L.; Xie, M.; Zhu, D.; Zhou, F.; Zhang, F.; Kim, D.; Fraser, K.; Kramer, L. D.; Seeman, N. C.; Dordick, J. S.; Linhardt, R. J.; Chao, J.; Wang, X. Designer DNA architecture offers precise and multivalent spatial pattern-recognition for viral sensing and inhibition. *Nat. Chem.* **2020**, *12*, 26−35.

(18) Cremers, G. A. O.; Rosier, B. J. H. M.; Meijs, A.; Tito, N. B.; van Duijnhoven, S. M. J.; van Eenennaam, H.; Albertazzi, L.; de Greef, T. F. A. Determinants of Ligand-Functionalized DNA Nanostructure-Cell Interactions. *J. Am. Chem. Soc.* **2021**, *143*, 10131−10142.

(19) Zhang, C.; Tian, C.; Guo, F.; Liu, Z.; Jiang, W.; Mao, C. DNA-Directed Three-Dimensional Protein Organization. *Angew. Chem., Int. Ed.* **2012**, *51*, 3382−3385.

(20) Sigl, C.; Willner, E. M.; Engelen, W.; Kretzmann, J. A.; Sachenbacher, K.; Liedl, A.; Kolbe, F.; Wilsch, F.; Aghvami, S. A.; Protzer, U.; Hagan, M. F.; Fraden, S.; Dietz, H. Programmable icosahedral shell system for virus trapping. *Nat. Mater.* **2021**, *20*, 1281−1289.

(21) Woehrstein, J. B.; Strauss, M. T.; Ong, L. L.; Wei, B.; Zhang, D. Y.; Jungmann, R.; Yin, P. Sub-100-nm metafluorophores with digitally tunable optical properties self-assembled from DNA. *Sci. Adv.* **2017**, *3*, No. e1602128.

(22) Rinker, S.; Ke, Y.; Liu, Y.; Chhabra, R.; Yan, H. Self-assembled DNA nanostructures for distance-dependent multivalent ligand-protein binding. *Nat. Nanotechnol.* **2008**, *3*, 418−422.
(23) Benton, D. J.; Wrobel, A. G.; Xu, P.; Roustan, C.; Martin, S. R.; Rosenthal, P. B.; Skehel, J. J.; Gamblin, S. J. Receptor binding and priming of the spike protein of SARS-CoV-2 for membrane fusion. *Nature* **2020**, *588*, 327−330.
(24) Klein, S.; Cortese, M.; Winter, S. L.; Wachsmuth-Melm, M.; Neufeldt, C. J.; Cerikan, B.; Stanifer, M. L.; Boulant, S.; Bartenschlager, R.; Chlanda, P. SARS-CoV-2 structure and replication characterized by in situ cryo-electron tomography. *Nat. Commun.* **2020**, *11*, 5885.
(25) Zhang, C.; Wang, Y.; Zhu, Y.; Liu, C.; Gu, C.; Xu, S.; Wang, Y.; Zhou, Y.; Wang, Y.; Han, W.; Hong, X.; Yang, Y.; Zhang, X.; Wang, T.; Xu, C.; Hong, Q.; Wang, S.; Zhao, Q.; Qiao, W.; Zang, J.; Kong, L.; Wang, F.; Wang, H.; Qu, D.; Lavillette, D.; Tang, H.; Deng, Q.; Xie, Y.; Cong, Y.; Huang, Z. Development and structural basis of a two-MAb cocktail for treating SARS-CoV-2 infections. *Nat. Commun.* **2021**, *12*, 264.
(26) Yang, Y.; Xu, Y.; Yang, Y.; Shi, Q.; Ward, A.; Wang, W. An infectious virus-like particle built on a programmable icosahedral DNA framework. *Chemrxiv* **2022**, DOI: 10.26434/chemrxiv-2022-20s93.
(27) Ke, Z.; Oton, J.; Qu, K.; Cortese, M.; Zila, V.; McKeane, L.; Nakane, T.; Zivanov, J.; Neufeldt, C. J.; Cerikan, B.; Lu, J. M.; Peukes, J.; Xiong, X.; Kräusslich, H.-G.; Scheres, S. H. W.; Bartenschlager, R.; Briggs, J. A. G. Structures and distributions of SARS-CoV-2 spike proteins on intact virions. *Nature* **2020**, *588*, 498−502.
(28) Koenig, P. A.; Das, H.; Liu, H.; Kümmerer, B. M.; Gohr, F. N.; Jenster, L. M.; Schiffelers, L. D. J.; Tesfamariam, Y. M.; Uchima, M.; Wuerth, J. D.; Gatterdam, K.; Ruetalo, N.; Christensen, M. H.; Fandrey, C. I.; Normann, S.; Tödtmann, J. M. P.; Pritzl, S.; Hanke, L.; Boos, J.; Yuan, M.; Zhu, X.; Schmid-Burgk, J. L.; Kato, H.; Schindler, M.; Wilson, I. A.; Geyer, M.; Ludwig, K. U.; Hällberg, B. M.; Wu, N. C.; Schmidt, F. I. Structure-guided multivalent nanobodies block SARS-CoV-2 infection and suppress mutational escape. *Science* **2021**, *371*, No. eabe6230.
(29) Cao, Y.; Wang, J.; Jian, F.; Xiao, T.; Song, W.; Yisimayi, A.; Huang, W.; Li, Q.; Wang, P.; An, R.; Wang, J.; Wang, Y.; Niu, X.; Yang, S.; Liang, H.; Sun, H.; Li, T.; Yu, Y.; Cui, Q.; Liu, S.; Yang, X.; Du, S.; Zhang, Z.; Hao, X.; Shao, F.; Jin, R.; Wang, X.; Xiao, J.; Wang, Y.; Xie, X. S. Omicron escapes the majority of existing SARS-CoV-2 neutralizing antibodies. *Nature* **2021**, *602*, 657−663.
(30) Sun, M.; Wu, Z.; Zhang, J.; Chen, M.; Lu, Y.; Yang, C.; Song, Y. Spherical neutralizing aptamer suppresses SARS-CoV-2 Omicron escape. *Nano Today* **2022**, *44*, 101499.
(31) Li, Q.; Nie, J.; Wu, J.; Zhang, L.; Ding, R.; Wang, H.; Zhang, Y.; Li, T.; Liu, S.; Zhang, M.; Zhao, C.; Liu, H.; Nie, L.; Qin, H.; Wang, M.; Lu, Q.; Li, X.; Liu, J.; Liang, H.; Shi, Y.; Shen, Y.; Xie, L.; Zhang, L.; Qu, X.; Xu, W.; Huang, W.; Wang, Y. SARS-CoV-2 501Y.V2 variants lack higher infectivity but do have immune escape. *Cell* **2021**, *184*, 2362−2371.
(32) Suzuki, R.; Yamasoba, D.; Kimura, I.; Wang, L.; Kishimoto, M.; Ito, J.; Morioka, Y.; Nao, N.; Nasser, H.; Uriu, K.; Kosugi, Y.; Tsuda, M.; Orba, Y.; Sasaki, M.; Shimizu, R.; Kawabata, R.; Yoshimatsu, K.; Asakura, H.; Nagashima, M.; Sadamasu, K.; Yoshimura, K.; Suganami, M.; Oide, A.; Chiba, M.; Ito, H.; Tamura, T.; Tsushima, K.; Kubo, H.; Ferdous, Z.; Mouri, H.; Iida, M.; Kasahara, K.; Tabata, K.; Ishizuka, M.; Shigeno, A.; Tokunaga, K.; Ozono, S.; Yoshida, I.; Nakagawa, S.; Wu, J.; Takahashi, M.; Kaneda, A.; Seki, M.; Fujiki, R.; Nawai, B. R.; Suzuki, Y.; Kashima, Y.; Abe, K.; Imamura, K.; Shirakawa, K.; Takaori-Kondo, A.; Kazuma, Y.; Nomura, R.; Horisawa, Y.; Nagata, K.; Kawai, Y.; Yanagida, Y.; Tashiro, Y.; Takahashi, O.; Kitazato, K.; Hasebe, H.; Motozono, C.; Toyoda, M.; Tan, T. S.; Ngare, I.; Ueno, T.; Saito, A.; Butlertanaka, E. P.; Tanaka, Y. L.; Morizako, N.; Sawa, H.; Ikeda, T.; Irie, T.; Matsuno, K.; Tanaka, S.; Fukuhara, T.; Sato, K. Attenuated fusogenicity and pathogenicity of SARS-CoV-2 Omicron variant. *Nature* **2022**, *603*, 700−705.
(33) Liu, L.; Wang, P.; Nair, M. S.; Yu, J.; Rapp, M.; Wang, Q.; Luo, Y.; Chan, J. F.-W.; Sahi, V.; Figueroa, A.; Guo, X. V.; Cerutti, G.; Bimela, J.; Gorman, J.; Zhou, T.; Chen, Z.; Yuen, K.-Y.; Kwong, P. D.; Sodroski, J. G.; Yin, M. T.; Sheng, Z.; Huang, Y.; Shapiro, L.; Ho, D. D. Potent neutralizing antibodies against multiple epitopes on SARS-CoV-2 spike. *Nature* **2020**, *584*, 450−456.
(34) Pinto, D.; Park, Y.-J.; Beltramello, M.; Walls, A. C.; Tortorici, M. A.; Bianchi, S.; Jaconi, S.; Culap, K.; Zatta, F.; De Marco, A.; Peter, A.; Guarino, B.; Spreafico, R.; Cameroni, E.; Case, J. B.; Chen, R. E.; Havenar-Daughton, C.; Snell, G.; Telenti, A.; Virgin, H. W.; Lanzavecchia, A.; Diamond, M. S.; Fink, K.; Veesler, D.; Corti, D. Cross-neutralization of SARS-CoV-2 by a human monoclonal SARS-CoV antibody. *Nature* **2020**, *583*, 290−295.
(35) Jiang, D.; Ge, Z.; Im, H.-J.; England, C. G.; Ni, D.; Hou, J.; Zhang, L.; Kutyreff, C. J.; Yan, Y.; Liu, Y.; Cho, S. Y.; Engle, J. W.; Shi, J.; Huang, P.; Fan, C.; Yan, H.; Cai, W. DNA origami nanostructures can exhibit preferential renal uptake and alleviate acute kidney injury. *Nat. Biomed. Eng.* **2018**, *2*, 865−877.
(36) Li, S.; Jiang, Q.; Liu, S.; Zhang, Y.; Tian, Y.; Song, C.; Wang, J.; Zou, Y.; Anderson, G. J.; Han, J.-Y.; Chang, Y.; Liu, Y.; Zhang, C.; Chen, L.; Zhou, G.; Nie, G.; Yan, H.; Ding, B.; Zhao, Y. A DNA nanorobot functions as a cancer therapeutic in response to a molecular trigger in vivo. *Nat. Biotechnol.* **2018**, *36*, 258−264.
(37) Jiang, S.; Ge, Z.; Mou, S.; Yan, H.; Fan, C. Designer DNA nanostructures for therapeutics. *Chem* **2021**, *7*, 1156−1179.
(38) Knappe, G. A.; Wamhoff, E.-C.; Read, B. J.; Irvine, D. J.; Bathe, M. In Situ Covalent Functionalization of DNA Origami Virus-like Particles. *ACS Nano* **2021**, *15*, 14316−14322.
(39) Liu, S.; Jiang, Q.; Zhao, X.; Zhao, R.; Wang, Y.; Wang, Y.; Liu, J.; Shang, Y.; Zhao, S.; Wu, T.; Zhang, Y.; Nie, G.; Ding, B. A DNA nanodevice-based vaccine for cancer immunotherapy. *Nat. Mater.* **2021**, *20*, 421−430.
(40) Du, S.; Cao, Y.; Zhu, Q.; Yu, P.; Qi, F.; Wang, G.; Du, X.; Bao, L.; Deng, W.; Zhu, H.; Liu, J.; Nie, J.; Zheng, Y.; Liang, H.; Liu, R.; Gong, S.; Xu, H.; Yisimayi, A.; Lv, Q.; Wang, B.; He, R.; Han, Y.; Zhao, W.; Bai, Y.; Qu, Y.; Gao, X.; Ji, C.; Wang, Q.; Gao, N.; Huang, W.; Wang, Y.; Xie, X. S.; Su, X.-d.; Xiao, J.; Qin, C. Structurally Resolved SARS-CoV-2 Antibody Shows High Efficacy in Severely Infected Hamsters and Provides a Potent Cocktail Pairing Strategy. *Cell* **2020**, *183*, 1013−1023.
(41) Xiang, Y.; Nambulli, S.; Xiao, Z.; Liu, H.; Sang, Z.; Duprex, W. P.; Schneidman-Duhovny, D.; Zhang, C.; Shi, Y. Versatile and multivalent nanobodies efficiently neutralize SARS-CoV-2. *Science* **2020**, *370*, 1479−1484.
(42) Wrapp, D.; De Vlieger, D.; Corbett, K. S.; Torres, G. M.; Wang, N.; Van Breedam, W.; Roose, K.; van Schie, L.; Hoffmann, M.; Pöhlmann, S.; Graham, B. S.; Callewaert, N.; Schepens, B.; Saelens, X.; McLellan, J. S.; McLellan, J. S. Structural Basis for Potent Neutralization of Betacoronaviruses by Single-Domain Camelid Antibodies. *Cell* **2020**, *181*, 1004−1015.

https://doi.org/10.1021/jacs.2c02764
J. Am. Chem. Soc. XXXX, XXX, XXX−XXX